Supplementary Information (SI) for Journal of Materials Chemistry A.

Supplementary Information
for
Robust Cu(0) active sites stabilized by high surface pH gradient for ultra-low potential HMF oxidation

Honglei Chen,[a] Yanming Li,[a] Zeyu Huang,[a] Lan Wang,[a,b] Changli Li,[a]* Jingfu He[a]*

a. School of Materials, Shenzhen Campus of Sun Yat-sen University, No. 66, Gongchang Road, Guangming District, Shenzhen, Guangdong 518107, P.R. China

b. School of Chemical Engineering, Sichuan University of Science and Engineering, Zigong 643000, People's Republic of China.

Changli Li* − Email: lichli5@mail.sysu.edu.cn

Jingfu He* − Email: hejf27@mail.sysu.edu.cn

1 Methods

1.1 Materials and chemicals.

Commercial Cu foam was purchased from Canrd Chemical Technology. Potassium hydroxide (analytical reagent, AR), hydrochloric acid (AR), acetone and ammonium formate (HPLC) were purchased from Macklin Chemical Reagent. Ethanol and Copper (II) Sulfate Pentahydrate were purchased from General-Ragent Chemical Reagent. 5-Hydroxymethyl-2-furaldehyde, Methanol (HPLC) were purchased from Aladdin Chemical Reagent, 5-Hydroxymethyl-2-furancarboxylic acid were purchased from Bide Chemical Reagent.

1.2 Synthesis of catalysts

1.2.1 Pretreatment of Cu foam (CF)

Copper foam was sonicated with acetone, 3 M HCl, absolute ethanol, and deionized water for 5 min respectively. Then, the cleaned copper foam was blowing dry with nitrogen.

1.2.2 Synthesis of Cu NSs

The Cu NSs was prepared by the electroplating process. In a typical process, 6.25 g $CuSO_4·5H_2O$, 2.5 mL absolute ethanol, deionized water, and appropriate H_2SO_4 were prepared into a 50 mL plating solution with a pH of 0.48. After sufficient ultrasonic uniformity, electroplating was carried out under a three-electrode system. The working electrode, counter electrode and reference electrode was CF (2 cm×3 cm×1.5 mm), graphite rod and Ag/AgCl, respectively. Operating at -20 mA for 600 s and then washed with ethanol and dried with nitrogen. Then, this CF was used as working electrode, Hg/HgO electrode was used as the reference electrode, the oxidation was completed under the CV test of the three-electrode system between -0.1 and 1.2 V vs RHE in 1M KOH for 5 cycles at a scan rate of 5 mV/s.

1.2.3 Synthesis of Cu NWs(3)

The cleaned and blow-dried CF (1 cm×1.5 cm×1.5 mm) was placed in a porcelain boat and air annealed in a muffle furnace. Set the temperature rise program of 10 degrees per minute from room temperature to 500°C and keep it for 12 hours, and then naturally cool down. The resulting sample was named 500°C-12h. After that, the sample was electroreduced by a three-electrode system. The electrolyte was CO2-satuated 0.1M $KHCO_3$, whose pH was 6.85. This CF was used as working electrode, AgCl electrode was used as the reference electrode, Pt electrode was used as the counter electrode, the reduction was at -1.1V vs AgCl for n hours, corresponding to Cu NWs(n).

1.2.4 Synthesis of Pt/CC

Carbon cloth was sonicated with isopropanol, ethanol and water for 10 min respectively. Then, the cleaned copper foam was dried under an infrared lamp. Prepare ink, containing 3mL isopropanol, 120uL Nafion, 1mL water and 20 mg Pt/C. After ultrasonic homogenization, spray it on a 3×3cm^2 carbon fiber cloth with a spray gun.

2 Characterization and tests

2.1 Characterization

The morphology and microstructure of the CF, Cu-CF and Cu_2O-CF were investigated SEM (Hitachi, SU5000). The high-resolution morphology of these materials was observed by TEM (FEI Tecnai G2 F20). XRD was employed on a Rigaku SmartLab SE diffractometer with a Cu Ka source. Diffraction data were collected for 2ɵ from 10 to 90 °. The Raman spectra were recorded at room temperature on a WiTech alpha 300R with an argon ion laser operating at 488 nm. The XPS was performed on an Thermo Scientific K-Alpha X-ray photoelectron spectrometer using Al as the excitation source (hv=1486.6eV). In-situ FT-IR measurements of HMF adsorption was carried out over Bruker infrared spectrometer (Transmission cell) in the reaction cell. The IR reaction cell was equipped without window and a typical three electrodes system was operated (Pt wire as counter electrode and Hg/HgO as reference electrode).

2.2 Electrochemical measurements

The linear sweep voltammetry (LSV) and cyclic voltammetry (CV) was recorded in an H-type electrochemical cell with 1 M KOH and various quantities of HMF at room temperature at a scanning rate of 5 mV/s. The synthesized Cu NSs or Cu NWs(n), a graphite rod, and a Hg/HgO electrode (1 M KOH) were utilized as the working, counter, and reference electrodes, respectively. The anode and cathode chambers were separated by a Nafion membrane. The recorded potential was normalized with respect to the reversible hydrogen electrode (RHE) according to the following procedure:

$$E_{RHE}=E^{\ominus}(Hg/HgO) + 0.059\times pH + 0.098. \quad (1)$$

ECSA was studied based on the electrochemical double-layer capacitance of various electrocatalysts at non-faradaic overpotentials. By plotting the difference of j between the anodic and cathodic sweeps (ja–jc) at 0.9 V vs. RHE against the scan rate, a linear trend was observed. The slope of the fitting line is equal to twice the geometric double layer capacitance (C_{dl}). The specific capacitance (C_s) for a flat surface is normally taken to be 40 μF/cm^2. Generally, the ECSA of the catalyst can be calculated by the following function:

$$\mathrm{ECSA} = C_{dl}/C_s \qquad (2)$$

2.3 Tandem configuration

The electrochemical test of tandem system is accomplished by double electrode system to realize cathodic oxygen reduction and anodic HMFOR. In this configuration, Cu NWs(3) acted as working electrode while Pt/CC served as couple electrode. The tandem system is designed based on H-cell to separate cathodic (0.1 M KOH) and anodic (1 M KOH with 50 mM HMF) electrolyte. The linear sweep voltammetry (LSV) curve was employed to record the current response at different cell voltage with scanning rate of 5 mV/s. To carry out bias-free tandem reaction, the applied cell voltage was set as 0 V. High purity O_2 was purged into the cathode electrolyte to supply.

2.4 HPLC analysis

HPLC (1260 Infinity II) with a UV detector was used to analyze HMF oxidation liquid phase products. The UV detector was adjusted to a wavelength of 265 nm. The mobile phase for HPLC was a mixture of ammonium formate and methanol, and the flow rate was 0.6 mL/min. A 4.6 mm×350 mm C18 column was used. The electrolyte was diluted to pH=13 before HPLC analysis. The quantification of HMF and its oxidation product was calculated based on the calibration curves of standard compounds with known concentrations. Specifically, each potential (0.1-0.7 for Cu NWs(3) and 0.2-0.7 for Cu NSs) was applied for one hour to quantitatively detect the liquid product (Figure 2b-c). The electrolyte was 1M KOH with 50mM HMF, and the electrolysis was operated in H-cell with AEM. The FE of products was calculated on the basis of the following equations:

$$\text{Faraday efficiency (\%)} = n_{\text{experimentally produced}} / n_{\text{theoretically produced}} \times 100 \qquad (3)$$

where n is the mole number of the substrate. The theoretically produced amount was calculated on the basis of

$$n_{\text{theoretically produced}} = Q/(n \times F) \qquad (4)$$

where Q is the transferred charge, n is the number of electrons transferred for each product molecule and F is Faraday’s constant (96485 C/mol).

3 Comsol Multiphysics Simulations

The electric field and concentration distribution of ions were simulated using the COMSOL Multiphysics finite-element based solver. The Butler-Volmer equation and Fick’s second law were applied to simulate the electrochemical kinetic process and ion diffusion process, the current-potential relationship and the ion concentration were obtained, respectively. The time dependence of the ion concentration and the current value is established by the above model, and the value corresponding to the time points close to the steady state is finally selected. In this model, the diffusion coefficients of substrate, product and other components were $7.2*10^{-9}$ cm^2/s, the reaction rate constant was 10^7. The operated potential and theoretical potential were 0.4 V and -0.1 V. The current density was simulated in the electrochemical module via Butler–Volmer equation. In detail, the anodic and cathodic charge transfer coefficients were both equal to 0.5. 2D continuum model was built in this work to represent the 3D structures of electrodes. Triangular meshes with normal size were used for all simulations and the area near the electrode surface is divided into more detailed grids. The HMF concentration and OH^- concentration were set to 50 mM and 1 M at the bulk boundary.

Supply Figures

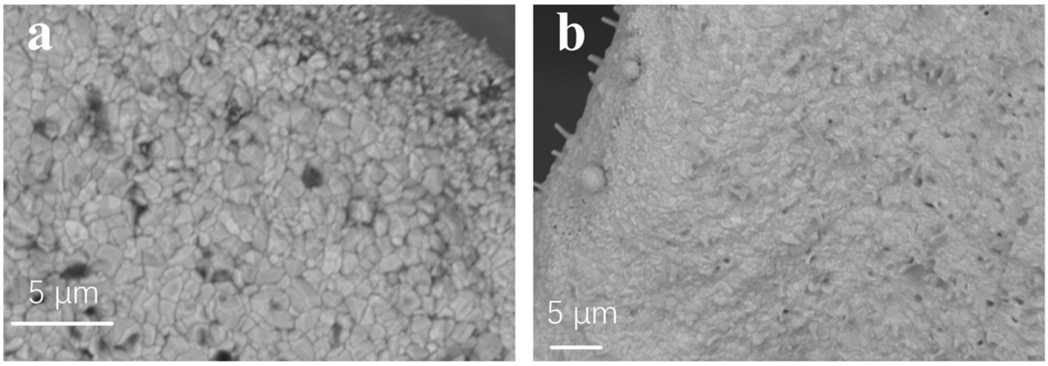

Figure S1. SEM images of 500C-12h/CF.

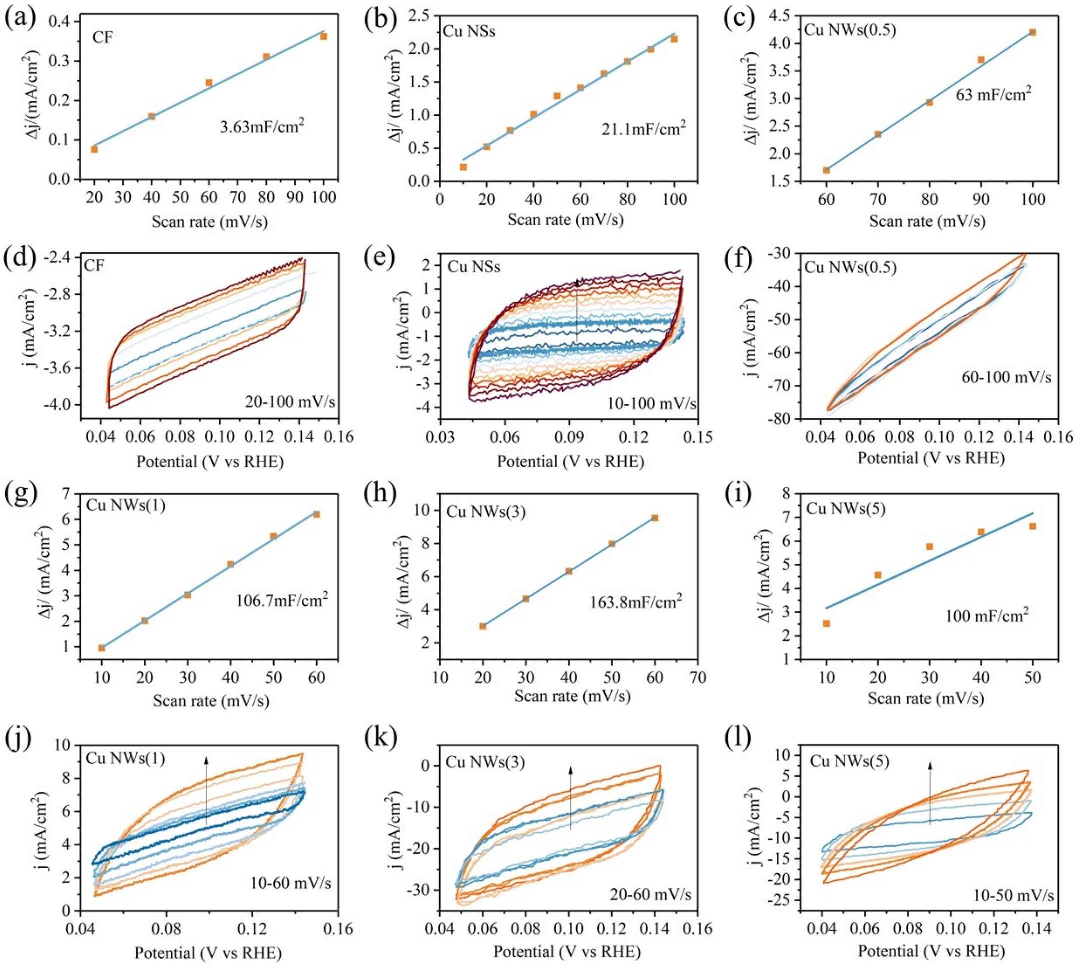

Figure S2. Capacitive currents at 0.09 V vs RHE as a function of the scan rate for (a) CF, (b) Cu NSs, (c) Cu NWs(0.5), (g) Cu NWs(1), (h) Cu NWs(3) and (i) Cu NWs(5). CV curves for (d) CF, (e) Cu NSs, (f) Cu NWs(0.5), (j) Cu NWs(1), (k) Cu NWs(3) and (l) Cu NWs(5) at different scan rates in the non-Faradaic region.

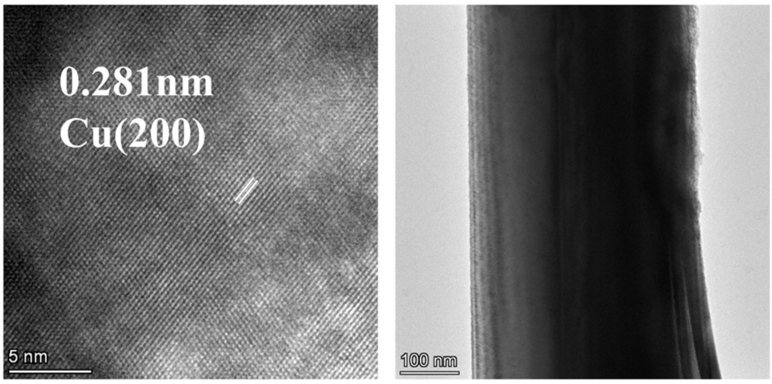

Figure S3. TEM images of Cu NWs(0.5).

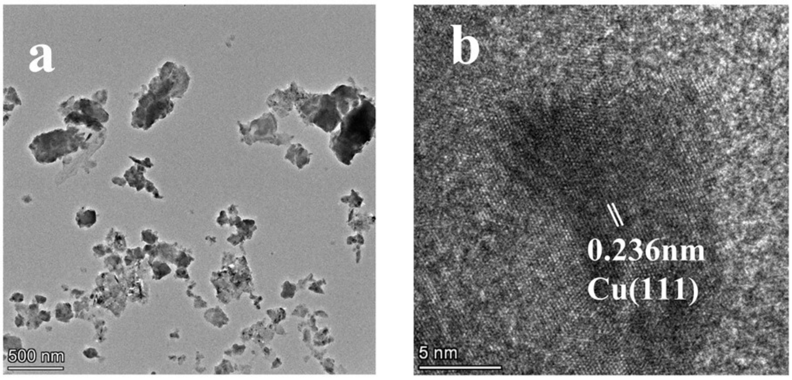

Figure S4. TEM images of Cu NSs.

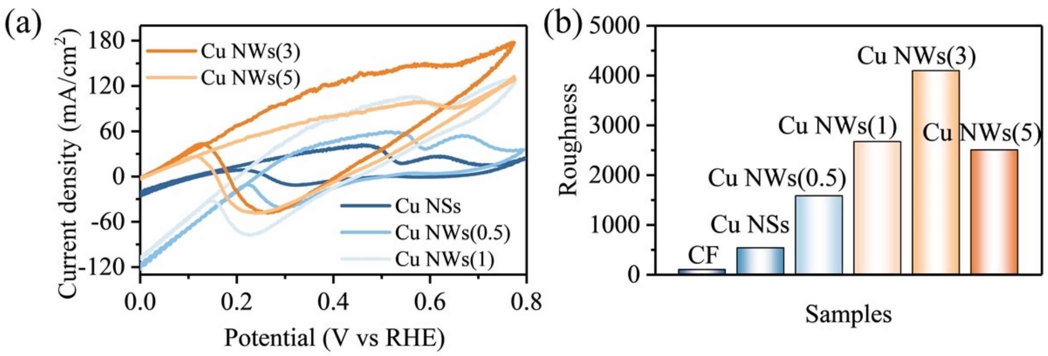

Figure S5. (a) CV curves of Cu NWs(0.5), Cu NWs(1), Cu NWs(3), Cu NWs(5) and Cu NSs in 1.0 M KOH with 50 mM HMF collected at 5 mV/s. (b) Roughness of CF, Cu NWs(0.5), Cu NWs(1), Cu NWs(2), Cu NWs(3), Cu NWs(5) and Cu NSs, related to Figure S2.

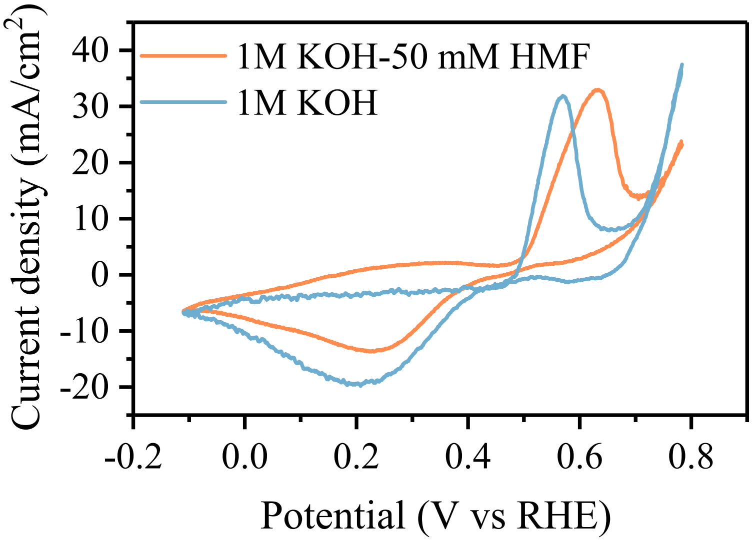

Figure S6. CV curves of CF in 1 M KOH with and without 50 mM HMF, the scan rate is 5 mV/s.

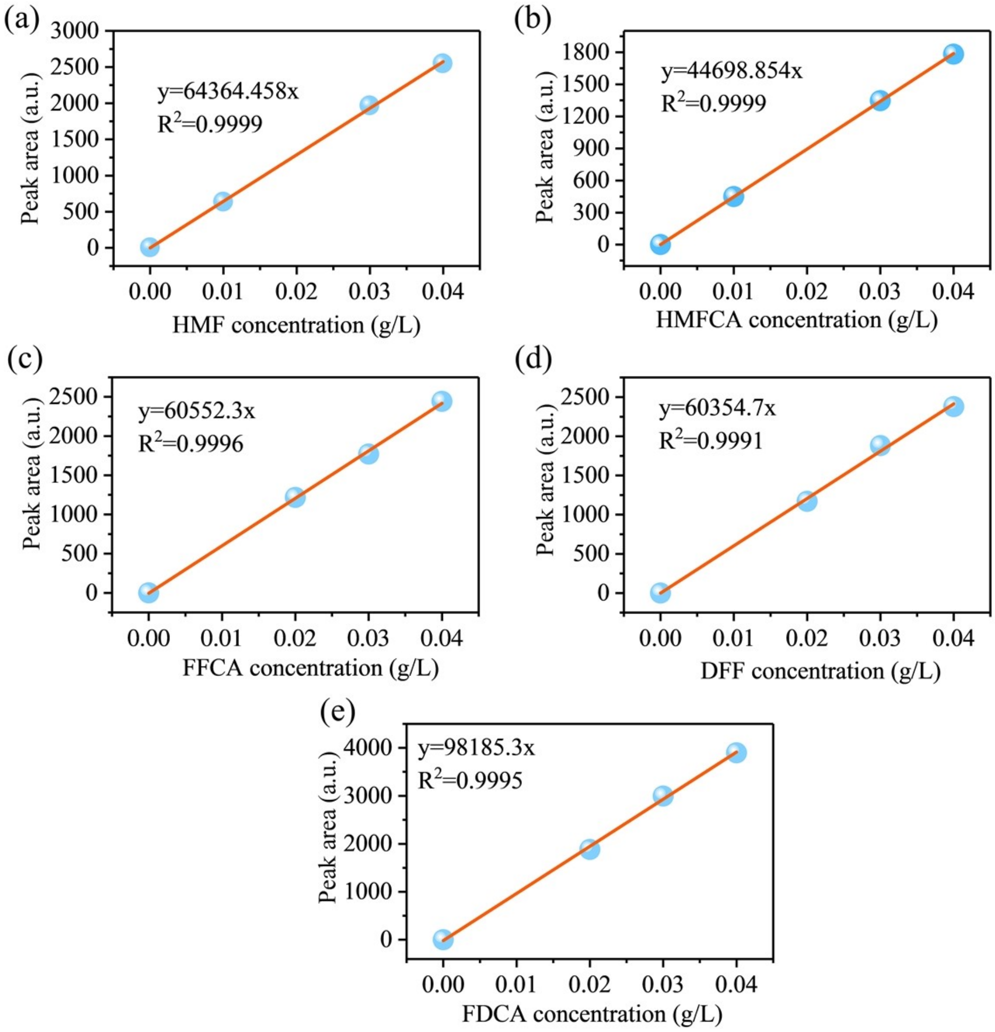

Figure S7. Calibration of the HPLC for (a) HMF. (b) HMFCA. (c) FFCA. (d) DFF. (e) FDCA.

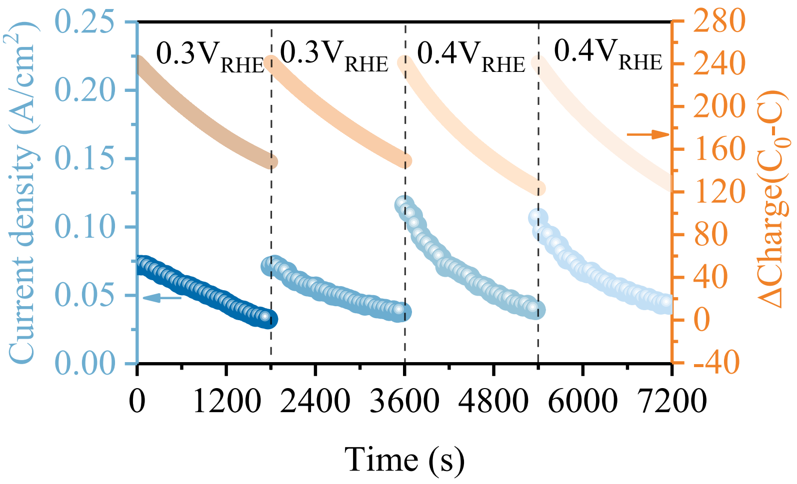

Figure S8. The i-t curves of the electrolysis on the Cu NWs(3) electrode at 0.3 V vs RHE and 0.4 V vs RHE in 1 M KOH with 50 mM HMF for 1 h, the dotted line represents the refreshing of electrolyte. The y-axis on the right represents the difference between the actual electric quantity and the theoretical electric quantity required for substrate consumption.

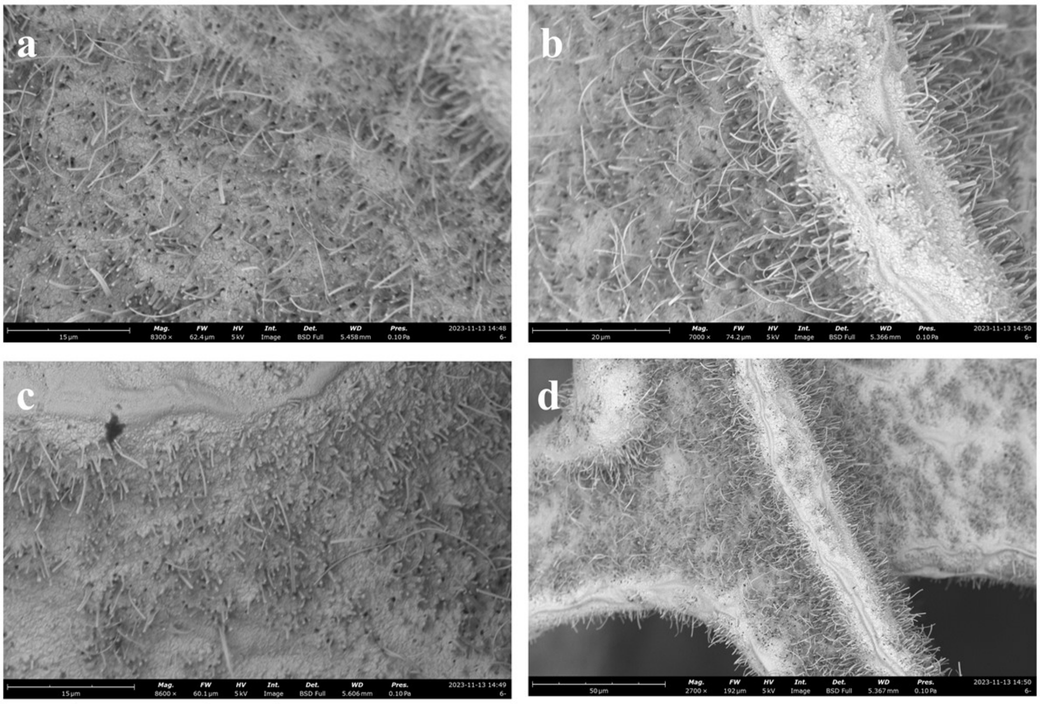

Figure S9. SEM images of Cu NWs(3) after electrolysis at 1M KOH with 50 mM HMF under 0.3 V vs RHE for 75 min.

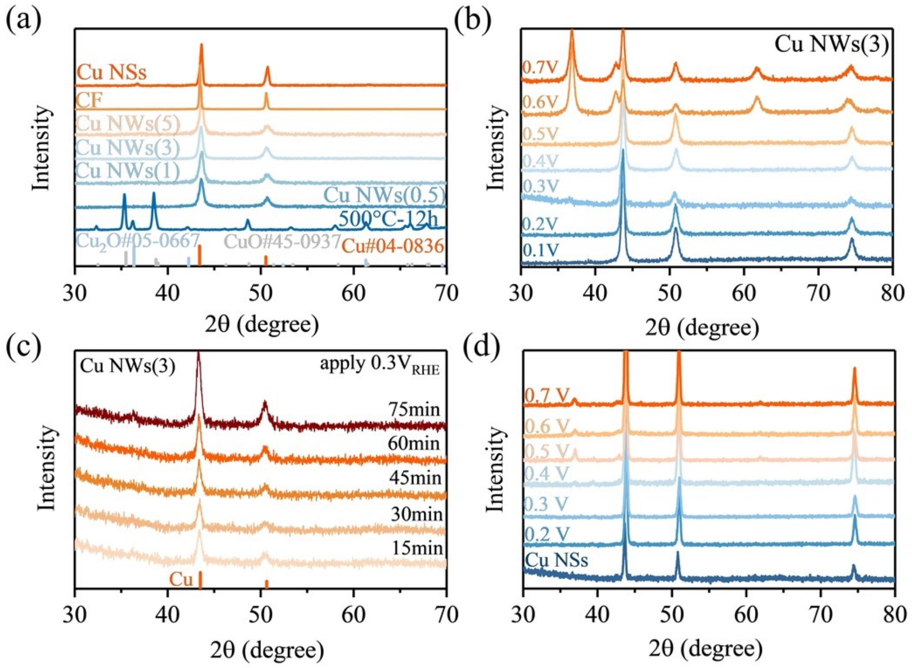

Figure S10. (a) XRD patterns for CF, Cu NSs, CF after thermolysis at 500°C for 12 h (named 500° C-12h), Cu NW(0.5), Cu NW(1), Cu NW(3) and Cu NW(5). (b) XRD patterns for Cu NWs(3) after electrolysis at 1M KOH with 50 mM HMF under 0.1 V, 0.2V, 0.3V, 0.4V, 0.5V, 0.6V and 0.7 V vs RHE for 1 h, respectively. (b) XRD patterns for Cu NWs(3) after electrolysis at 1M KOH with 50 mM HMF under 0.3 V vs RHE for 15min, 30min, 45min, 60min and 75min. (d) XRD patterns for Cu NSs after electrolysis at 1M KOH with 50 mM HMF under 0.2V, 0.3V, 0.4V, 0.5V, 0.6V and 0.7 V vs RHE for 1 h, respectively.

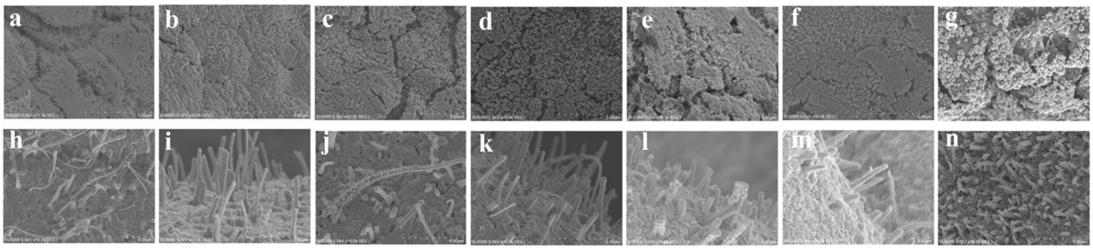

Figure S11. SEM images of (a) Cu NSs; SEM images of (b) Cu NSs after electrolysis at 1 M KOH with 50 mM HMF under 0.2 V vs RHE for 1 h; (c) Cu NSs after electrolysis at 1 M KOH with 50 mM HMF under 0.3 V vs RHE for 1 h; (d) Cu NSs after electrolysis at 1 M KOH with 50 mM HMF under 0.4 V vs RHE for 1 h; (e) Cu NSs after electrolysis at 1 M KOH with 50 mM HMF under 0.5 V vs RHE for 1 h; (f) Cu NSs after electrolysis at 1 M KOH with 50 mM HMF under 0.6 V vs RHE for 1 h; (g) Cu NSs after electrolysis at 1 M KOH with 50 mM HMF under 0.7 V vs RHE for 1 h. (h) Cu NWs(3) after electrolysis at 1 M KOH with 50 mM HMF under 0.1 V vs RHE for 1 h; (i) Cu NWs(3) after electrolysis at 1 M KOH with 50 mM HMF under 0.2 V vs RHE for 1 h; (j) Cu NWs(3) after electrolysis at 1 M KOH with 50 mM HMF under 0.3 V vs RHE for 1 h; (k) Cu NWs(3) after electrolysis at 1 M KOH with 50 mM HMF under 0.4 V vs RHE for 1 h; (l) Cu NWs(3) after electrolysis at 1 M KOH with 50 mM HMF under 0.5 V vs RHE for 1 h; (m) Cu NWs(3) after electrolysis at 1 M KOH with 50 mM HMF under 0.6 V vs RHE for 1 h; (n) Cu NWs(3) after electrolysis at 1 M KOH with 50 mM HMF under 0.7 V vs RHE for 1 h.

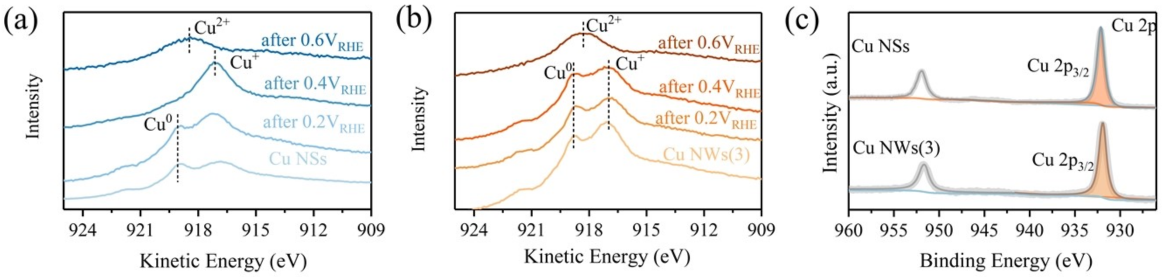

Figure S12. Auger electron spectra of (a) Cu NSs and (b) Cu NWs(3) after electrolysis in 1M KOH with 50 mM HMF at 0.2 V, 0.4 V and 0.6 V for 1h, respectively. (c)XPS spectra of Cu NSs and Cu NWs(3), Cu 2p.

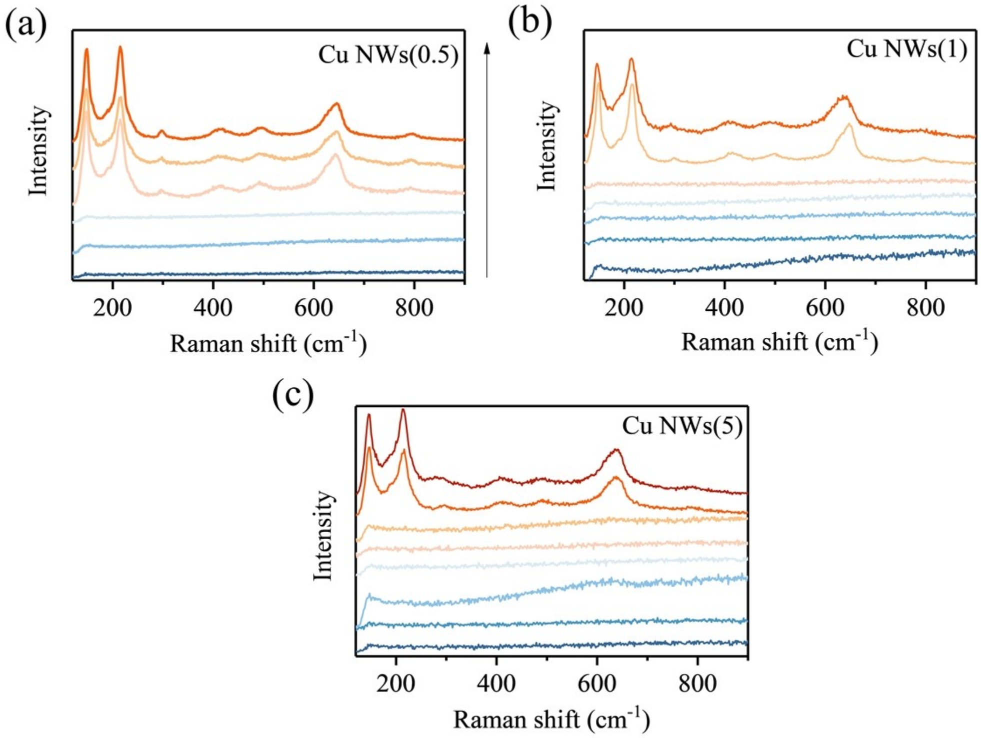

Figure S13. In situ Raman spectra 100–900 cm^{-1} of HMF oxidation reactions on (a) Cu NWs(0.5) at 0.2–0.7 V, the dark line is at OCP condition. In situ Raman spectra 100–900 cm^{-1} of HMF oxidation reactions on (b) Cu NWs(1) at 0.1–0.7 V. In situ Raman spectra 100–900 cm^{-1} of HMF oxidation reactions on (c) Cu NWs(5) at 0.1–0.7 V, the dark line is at OCP condition.

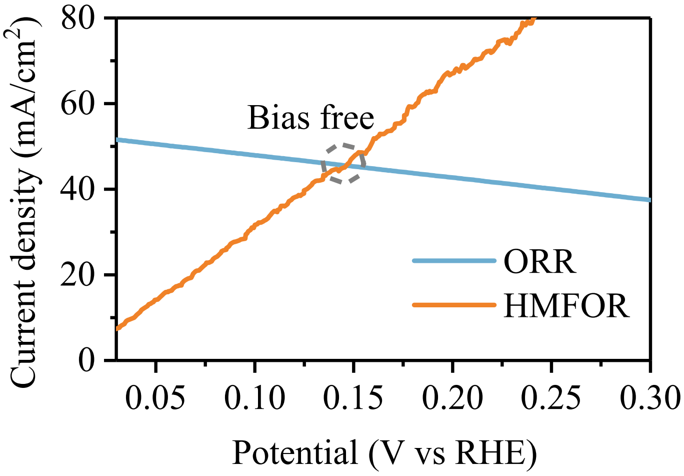

Figure S14. LSV curves of anodic HMFOR of Cu NWs(3) in the 1 M KOH with 50 mM HMF electrolyte and cathodic ORR of Pt/CC in the O_2-satuated 0.1 M KOH electrolyte. The point where the two intersect means the bias free condition.

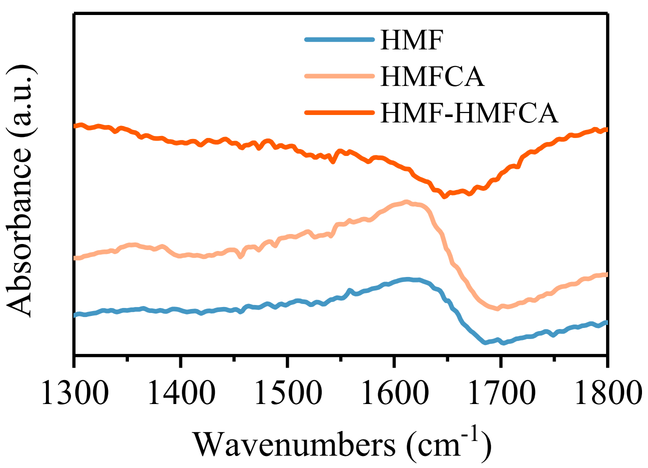

Figure S15. FT-IR spectra of Cu NWs(3) in the 1 M KOH electrolyte with HMF, HMFCA and HMF+HMFCA at OCP condition.

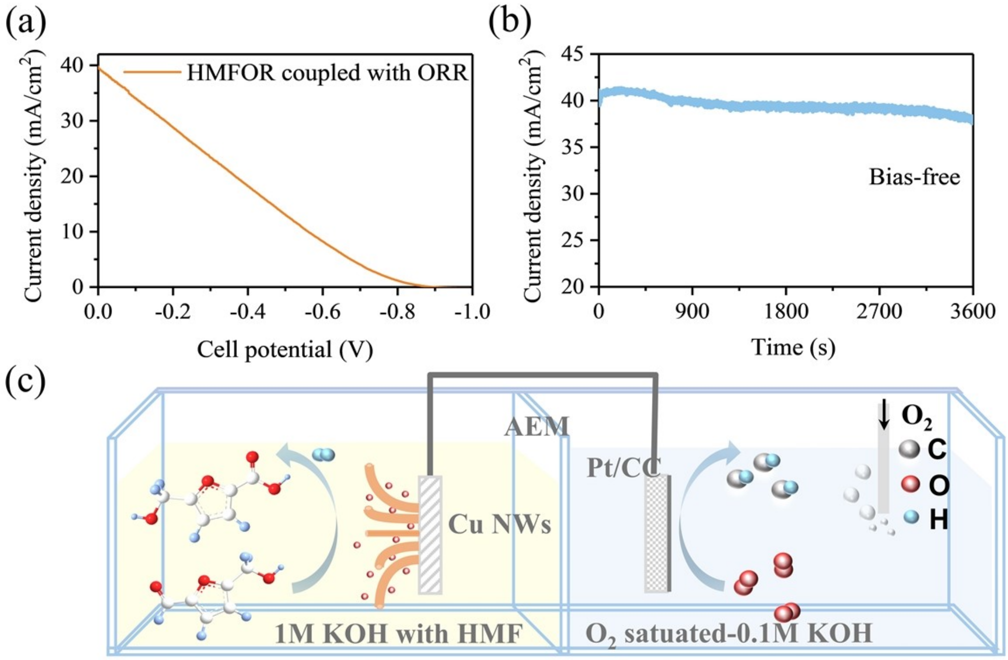

Figure S16. (a) LSV curves of integrate system; (b) I-t test of coupled system under bias-free condition. (c) The schematic diagram of the bias-free fuel cell composed of cathodic ORR by Pt/CC and anodic HMFOR.

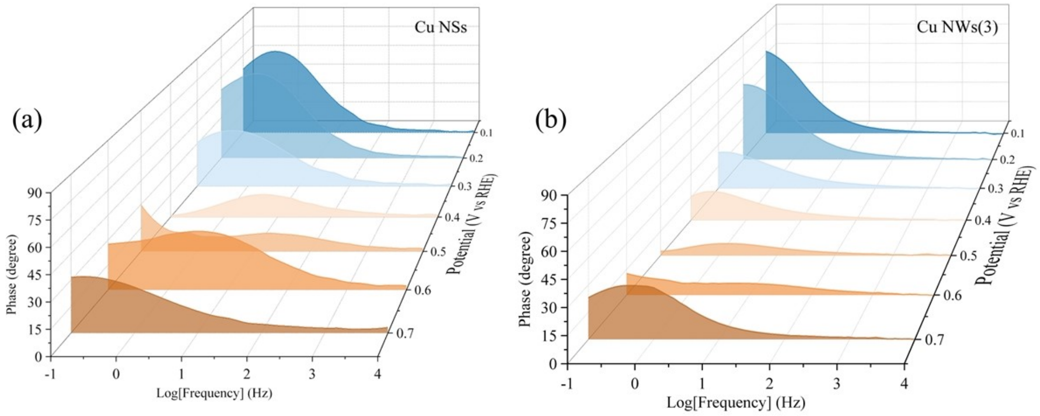

Figure S17. Bode plots of (a) Cu NSs and (b) Cu NWs(3) for HMFOR (1M KOH with 50 mM HMF) during 0.1 V to 0.7 V.

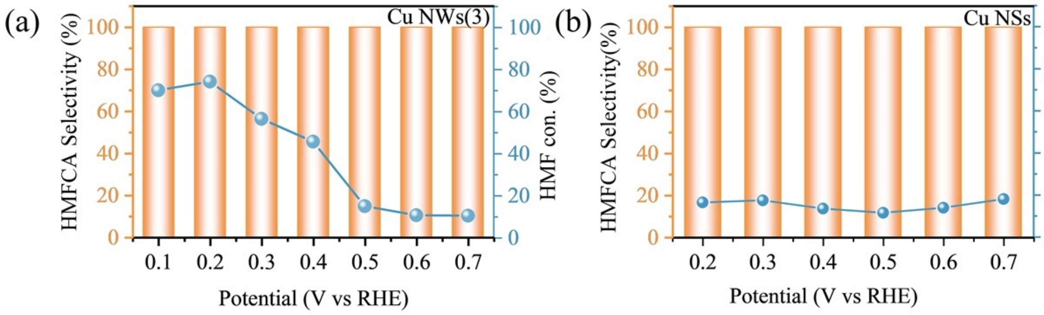

Figure S18. The selectivity and HMF conversion rate of Cu NWs(3) and Cu NSs during 0.1 V to 0.7 V.

Table S1 Summary of the low potential organic oxidation performance by Cu-based catalysts in 1M KOH.

Anode	**Oxidation substrate**	**Onset potential @ 1 mA/cm^2**	**Potential when oxidation current begins to decay**	**Ref**
Cu	1M HCHO	0.025V	0.5V	Energy Environ.Sci., 2023,16, 2696-2704
Cu_2O	1M CH_3CHO	0.5V	0.48V	Energy Environ. Sci., 2023,16, 2696-2704
Pt-Cu	0.2M FF	0.02V	0.23V	Energy Environ. Sci., 2023,16, 2696-2704
Cu	0.2M FF	0.04V	0.27V	Chem. Commun., 2023, 59, 6837
CF@Cu-NS	0.05M HCHO	-0.07V	0.45V	Angew. Chem. Int. Ed. 2023, 62, e202302950
Cu/CF	0.2M FF	0.12V	0.35V	Energy Environ. Sci., 2022,15, 4175-4189
CuAgglv/Cu	0.2M FF	0.11V	0.38V	Energy Environ. Sci., 2022,15, 4175-4189
OD-Cu	0.2M FF	0.14V	0.38V	Energy Environ. Sci., 2022,15, 4175-4189
Cu NPs/Cu	0.2M FF	0.21V	0.41V	Energy Environ. Sci., 2022,15, 4175-4189
MV Cu	0.05M FF	0.02V	0.48V	Adv. Mater. 2023, 2304203Nat. Catal. 2022, 5, 66.
Cu-modified glass carbon	0.05M HMF	0.15V@0.1mA/cm^2	0.38V	Nat. Catal., 2022, 5, 66-73
Cu-modified glass carbon	0.05M FF	0.25V	0.42V	Nat. Catal., 2022, 5, 66-73

Cu_xO@CF	0.1M HCHO	-0.05V	0.32V	Chem 2023, 9, 963–977
CF	0.1M HCHO	0.15V	0.38V	Chem 2023, 9, 963–977
CuAu	0.2M FF	0.12V	0.41V	ACS Appl. Mater. Interfaces 2023,15, 37477−37485
CuAg	0.2M FF	0.07V	0.38V	ACS Appl. Mater. Interfaces 2023,15, 37477−37485
CuPd	0.2M FF	0.05V	0.42V	ACS Appl. Mater. Interfaces 2023,15, 37477−37485
CuPt	0.2M FF	0.09V	0.37V	ACS Appl. Mater. Interfaces 2023,15, 37477−37485
CF	0.2M FF	0.16V	0.38V	ACS Appl. Mater. Interfaces 2023,15, 37477−37485
Cu	0.05M FF	0.02V	0.38V	Adv. Funct. Mater. 2024, 2404105
Rh_1Cu	0.03M FF	0.01V	0.42V	Angew. Chem. 2023, 135, e202304852
Cu needles	0.05M HMF	0.05V	0.4V	Nat. Commun. 2023, 14,8395
Cu NWs(3)	0.05M HMF	0V	0.6V	This work